American Mineralogist, Volume 96, pages 1467–1474, 2011

Thermodynamic properties of alloys of gold-74/palladium-26 with variable amounts of iron and the use of Au-Pd-Fe alloys as containers for experimental petrology

J. Brian Balta,* John R. Beckett, and Paul D. Asimow

Department of Geological and Planetary Sciences, California Institute of Technology, Pasadena, California 91125, U.S.A.

Abstract

Iron oxide-alloy equilibration experiments were conducted in H_2-CO_2 gas mixtures at 1 atm and 1125–1240 °C using strips of $Au_{74}Pd_{26}$ (wt%) and produced Au-Pd-Fe alloys with 0.03–13 wt% iron. A thermodynamic calibration for the mixing of $Au_{74}Pd_{26}$ with iron using an asymmetric regular solution leads to $W_{G\text{-}Fe} = -45.0 \pm 1.8$ kJ/mol and $W_{G\text{-}AuPd} = +19.5 \pm 7.7$ kJ/mol (1σ). Internal oxidation of iron was observed in a reversal experiment, suggesting that oxygen can be transferred across capsule boundaries during high-temperature experiments. This thermodynamic calibration is applicable to a wide range of oxygen fugacities and iron activities relevant to petrological and metallurgical applications at 1 atm and, as previous studies suggest excess volumes in this system are small, it can also be used to predict Fe activities in experiments at elevated pressure (up to 3 GPa). By pre-doping Au-Pd capsules to match Fe activities expected for the sample during an experiment, it is possible to maintain samples with little to no loss of iron. Pre-saturation of the capsule also provides a method for controlling the oxygen fugacity of samples if no formal oxygen buffer is available.

Keywords: Gold-palladium, capsules, iron, internal oxidation

Introduction

Understanding rock-forming processes in planetary bodies requires production of equilibrated samples covering a considerable range of temperatures, pressures, and compositions. Investigation of high-temperature and high-pressure metamorphism or melting of rocks presents special challenges because of the potential for interactions between the sample and its surroundings. Often, an experimental charge is encapsulated in a precious metal with a high melting point, such as Pt, Au, or Ag (e.g., Chou 1986; Kawamoto and Hirose 1994), but under conditions of geologic interest, these materials can interact with the sample and provide a conduit for interactions between the sample and the external medium.

For volatile-bearing experiments at low temperatures, gold capsules are commonly used, as this metal has a low diffusivity for hydrogen and other volatile elements (e.g., Wyllie and Tuttle 1961; Chou 1986; Truckenbrodt and Johannes 1999), but the relatively low melting point of Au makes it inappropriate for many problems relevant to the Earth's interior. Au-Pd alloys melt at higher temperatures than pure Au (Okamoto and Massalski 1985), but retain the desirable property of slow hydrogen diffusion (e.g., Maestas and Flanagan 1973). Unfortunately, Au-Pd alloys can also dissolve large amounts of Fe from a sample while at high temperature, making it difficult to establish equilibrium or to interpret the observed phase chemistry (e.g., Hall et al. 2004). The use of Au-Pd alloys to enclose Fe-bearing samples therefore requires understanding the issue of Fe solubility.

Iron solubility in Pt, a commonly used container material in experimental petrology, has long been a problem, and approaches similar to those used to mitigate Fe-loss to Pt capsules may also be applicable to Au-Pd capsules. Commonly applied techniques include graphite capsule liners to separate the sample from the container (e.g., Arndt 1976; Harrison 1981; Médard et al. 2008), restricting experiments to highly oxidizing conditions where the Fe solubility is low (e.g., Hall et al. 2004), and pre-doping of the container with Fe before use (e.g., Grove 1981; Aubaud et al. 2008). In principle, Fe-doping is the most flexible of these mitigation methods. Graphite liners or highly oxidizing environments limit the redox conditions that can be explored (and may contaminate the sample with carbon), whereas Fe contents of pre-doped containers can, in principle, be prepared to match a wide variety of conditions. In practice, however, pre-saturation is a Goldilocks problem. Just the right amount of Fe must be introduced; if too much Fe is introduced, the sample will gain Fe from the container; if too little Fe is introduced there will be Fe loss to the container. Furthermore, oxygen fugacity changes can be imposed on capsules from elsewhere in the assembly, such as from the heating element, making control even more difficult. Previous approaches to this problem for Au-Pd alloys have been largely ad hoc. For example, several authors, including Gaetani and Grove (1998), Kägi et al. (2005), Aubaud et al. (2008), and Botcharnikov et al. (2008) prepared Au-Pd capsules by first pre-saturating them in a gas mixing furnace at 1 atm using liquids similar to the ones expected at high pressure. This step adds Fe to the capsule material, but locating the conditions at 1 atm needed to saturate Au-Pd with the proper amount of Fe for a high-pressure experiment is an empirical and arduous process. Moreover, even after the correct 1 atm pre-doping conditions are determined for one high-pressure experiment, these conditions will differ from those needed for the next experiment in

* Present address: Department of Earth and Planetary Sciences, University of Tennessee-Knoxville, Knoxville, Tennessee 37909, U.S.A. E-mail: jbalta@utk.edu

0003-004X/11/0010–1467$05.00/DOI: 10.2138/am.2011.3637

ways that are difficult to predict due to other variables such as the presence of volatiles or compositional changes occurring during the experiment.

Kessel et al. (2001) presented a detailed calibration for the dissolution of Fe in Pt capsules and procedures by which Pt capsules for high-pressure experiments could be pre-saturated under ambient pressure using Fe-oxide-alloy equilibration to match the necessary alloy composition. Briefly, the basic approach is to use a thermodynamic calculator such as MELTS to predict the activity of Fe in a sample under the desired experimental conditions. This calculated activity is then converted to a target Pt-Fe alloy composition for pre-saturation by preparing and applying a calibration for the thermodynamic properties of the Pt-Fe system. Finally, the Pt-Fe alloy model is combined with the thermodynamic properties of the appropriate Fe-oxide to yield the redox conditions at ambient pressure that lead to the desired Fe content of the container for the desired sample bulk composition and run conditions. The approach of Kessel et al. (2001) is, in principle, equally applicable to Au-Pd-Fe alloys. Thermodynamic calculators such as MELTS or Thermocalc are available to calculate the activity of Fe in silicate phases, but there are no activity-composition data available for ternary Au-Pd-Fe alloys except along the bounding binaries. An alloy of $Au_{74}Pd_{26}$ was selected (composition on a weight basis), close to the commonly used $Au_{75}Pd_{25}$ alloy. Equilibration experiments were conducted to determine activity-composition relationships along the pseudo-binary join between this alloy and pure Fe for temperatures in the range 1125–1240 °C. We compare our results to the Au-Pd-Fe model of Barr and Grove (2010), which is nominally derived from the binaries but also postulates a "misfit parameter" to account for errors in Fe-partitioning caused by describing the thermodynamic properties of Au-Pd-Fe ternary alloys and silicate liquids using simplified solution models. Finally, we illustrate the potential of this technique by predicting the appropriate alloy compositions for a Kilauea basalt over a broad range of temperature and redox conditions and matching these predictions with the corresponding conditions at 1 atm under which the desired alloy compositions can be achieved by equilibrating the Au-Pd-Fe capsule with an iron oxide.

METHODS

We used a vertically mounted Deltech DT-31 $MoSi_2$-element gas-mixing furnace and controlled the f_{O_2} using H_2-CO_2 gas mixtures. EMFs were measured using an yttria-doped zirconia solid electrolyte oxygen sensor (SIRO2; Ceramic Oxide Fabricators) calibrated at the fixed points established by air and the iron-wüstite buffer. Oxygen sensor readings were maintained to within ±3 mV under oxidizing conditions and ±1 mV under reducing conditions, which translates to log f_{O_2} values within ±0.1 or better (1σ). For experiments conducted at 1190 and 1240 °C, we used an oxygen sensor with a gravity feed internal electrode. For 1125 °C, this arrangement failed to produce EMFs consistent with the Nernst equation due to inadequate electrical contact (e.g., Beckett and Mendybaev 1997). Under these conditions, f_{O_2} at 1200 °C was determined using the oxygen sensor, then the f_{O_2} was converted to the corresponding volume % CO_2 in an H_2-CO_2 gas mixture using the tables of Deines et al. (1974) and finally [also via Deines et al. (1974)], the f_{O_2} at 1125 °C for this same volume % CO_2 was determined. Temperatures were measured using a type S (Pt-$Pt_{90}Rh_{10}$) thermocouple calibrated against the melting point of gold and are expected to be accurate and constant to ±3 °C (1σ).

For each experiment, the sample was prepared by cutting a ~1 × 2 mm strip of 200 μm thick alloy foil of laboratory grade $Au_{74}Pd_{26}$ (as wt%; analyzed composition given in Table 1). The strip was packed in Fe_2O_3 (Puratronic, Alfa Aesar), compressed into a 7 mm diameter pellet without a binding agent, placed into a ~2 cm diameter by 3 cm long alumina crucible, and suspended in the hot spot of the Deltech furnace (Chamberlin et al. 1994). Most of the experiments were conducted at 1190 °C, which is above the liquidus of common basaltic liquids often used for pre-saturation, with additional experiments at 1125 and 1240 °C. A maximum temperature of 1240 °C was chosen because the 1 atm solidus of the Fe-free alloy $Au_{74}Pd_{26}$ was intersected at ~1250 °C.

All experiments were conducted at redox conditions such that the stable solid oxide was either magnetite or wüstite. Experiments were run for a minimum of 48 h for the two higher temperatures and 72 h at 1125 °C. These times were sufficient to homogenize the Au-Pd-Fe alloys, consistent with homogenization time scales expected based on known diffusivities for solid Pd-Fe alloys (e.g., van Dal et al. 2000; Iijima and Yamazaki 2005) and also sufficient to fully convert the oxide pellet to either wüstite or magnetite from the initial hematite powder. Each experiment was terminated by removing the crucible through the top of the furnace and cooling it in ambient air. Cooling times were on the order of tens of seconds, sufficiently rapid that no obvious conversion of wüstite or magnetite to hematite (or magnetite) was observed. Moreover, no zoning was observed in electron microprobe analyses of the run product alloys, either near oxide-alloy interfaces or within the alloy strips.

TABLE 1. Experimental results

Run no.	T (°C)	Time (h)	Log (f_{O_2})	Fe oxide phase*	X_{Au}^{alloy}	X_{Pd}^{alloy}	X_{Fe}^{alloy}	$X_{Pd}^{alloy}/X_{Au}^{alloy}$	γ_{Fe}^{alloy}†
1	1190	70	–6.50	Magnetite	0.593(3)	0.390(2)	0.014(2)	0.658	0.029
2	1190	52	–6.75	Magnetite	0.592(2)	0.398(3)	0.017(1)	0.658	0.035
3	1190	69¾	–8.85	Magnetite	0.543(5)	0.356(3)	0.099(3)	0.657	0.151
4	1190	70	–9.75	Wüstite	0.494(5)	0.326(4)	0.178(2)	0.660	0.273
5	1190	71½	–10.50	Wüstite	0.455(8)	0.304(5)	0.244(2)	0.667	0.531
6	1190	61	–5.00	Magnetite	0.599(3)	0.397(2)	0.0021(6)	0.663	0.020
7	1190	72	–11.00	Wüstite	0.422(3)	0.277(2)	0.300(3)	0.655	0.817
8	1190	48	–3.90	Magnetite	0.603(3)	0.394(3)	0.0003(3)	0.653	0.029
8R‡					0.602(2)	0.395(2)	0.0004(7)	0.659	0.021
9	1190	69	–7.50	Magnetite	0.578(2)	0.382(1)	0.039(1)	0.661	0.049
10	1125	96	–10.50	Magnetite	0.488(2)	0.323(2)	0.188(1)	0.661	0.252
11	1240	62	–8.75	Wüstite	0.518(3)	0.346(2)	0.130(2)	0.667	0.220
12	1240	66	–9.50	Wüstite	0.460(8)	0.317(7)	0.217(2)	0.690	0.346
13	1125	82	–11.10	Wüstite	0.468(3)	0.304(1)	0.227(2)	0.650	0.450
14	1190	48	–8.25	Magnetite	0.565(2)	0.368(2)	0.066(1)	0.651	0.091
15	1240	50	–7.50	Magnetite	0.564(5)	0.371(4)	0.063(2)	0.658	0.080
16	1125	73½	–9.00	Magnetite	0.562(2)	0.368(2)	0.069(1)	0.656	0.069
Start					0.599(4)	0.400(4)	0.0006(8)	0.667	

Note: 1σ errors (given in parentheses) are calculated from 10–20 electron microprobe analyses of the product alloy.

* Identity of iron oxide observed in run products. Hematite was used to form all pellets prior to insertion in the furnace. Only a single oxide phase was observed in run products.

† Activity coefficient determined from activity of Fe at that temperature and the oxygen fugacity and measured Fe content in the alloy (see text).

‡ See entries under experiments 7 and 8 for the run conditions and compositions of separate Fe-free alloys run with the 8R alloy. An Fe-free alloy was placed in a hematite pellet and exposed to reducing conditions (run 7), quenched, extracted from the wüstite pellet produced during the experiment, placed in a new hematite pellet, and exposed to oxidizing conditions (run 8).

To confirm equilibrium, a reversal experiment was conducted by placing two strips in an iron oxide pellet and equilibrating them under reducing conditions, setting aside one strip from this initial experiment for analysis, and placing the second strip together with a fresh Fe-free strip for comparison into a new hematite pellet, and exposing the pellet to oxidizing conditions where the expected equilibrium Fe content of the alloy was much lower than in the first equilibration step.

Completed sample strips were removed from their pellets and cut into three roughly triangular pieces, one of which was stored for reference. Strips intended for analysis were mounted in epoxy, with one triangular piece laid flat in the plane of the section and the other roughly perpendicular to it, and polished using alumina and diamond pastes. Samples were carbon coated and analyzed using the JEOL JXA-8200 electron microprobe at Caltech in wavelength-dispersive mode. Samples were analyzed using a focused (0 µm setting) beam with an accelerating voltage of 15 kV and currents of 30–40 nA. Carbon-coated, metallic Fe, Au, and Pd were used as standards. Count times of 20 s were used on peak and 10 s off peak and between 10 and 25 spots were analyzed for each sample split between the two foil sections. The identity of the oxide present in each run product (wüstite vs. magnetite) was confirmed through semi-quantitative analysis of iron. No attempt was made to quantitatively determine the stoichiometry.

RESULTS

During an experiment, the initially Fe-free Au-Pd alloy reacts with the surrounding Fe-oxide and vapor to produce a ternary Au-Pd-Fe alloy. Observed alloy compositions vary between 0.03 and 30 mol% Fe; run conditions and the alloy compositions are given in Table 1 and displayed as a function of $\log f_{O_2}$ in Figure 1. For each temperature, the mole fraction of Fe(X_{Fe}^{alloy}) is a smooth function of $\log f_{O_2}$, and, with the exception of run 12, Pd/Au ratios in the alloys, 0.660 ± 0.010 (molar) are consistent with the observed Pd/Au of the Fe-free starting material (0.668 ± 0.011) suggesting negligible fractionation of Au from Pd through differential volatilization or differing solubilities in the coexisting Fe-oxide. Run 12, the most reduced experiment at the highest temperature, shows an elevated Pd content relative to Au (Pd/Au = 0.69), suggesting Au loss relative to Pd during the experiment, possibly to the wüstite. The activity-composition relationship determined from this experiment is, however, consistent with expectations based on the results for all of our other experiments and, therefore, run 12 was included in the modeling discussed below.

The basic objective of the experiments was to establish the thermodynamic properties of a suite of Au-Pd-Fe alloys by equilibrating them with wüstite or magnetite, phases whose thermodynamic properties are known, and then inverting the measured alloy compositions to obtain the activity coefficient of Fe in the alloy. Neither wüstite nor magnetite is stoichiometric under the experimental conditions of this study. For magnetite, deviations from nominal Fe_3O_4 stoichiometry can be neglected for the conditions of these experiments (e.g., Dieckmann 1982), but for wüstite, the Fe/O ratio of the oxide must be explicitly considered (Darken and Gurry 1945).

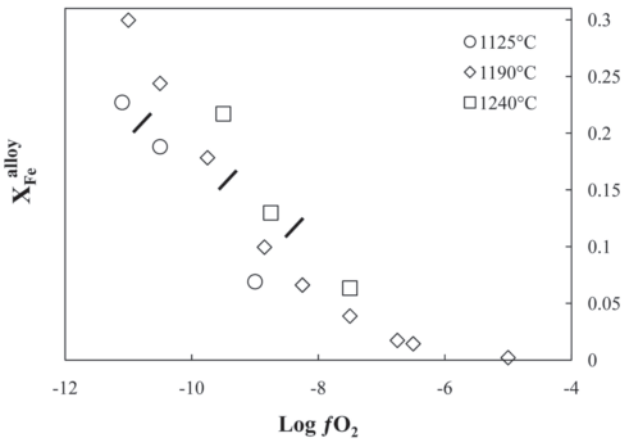

FIGURE 1. Mole fraction of Fe (X_{Fe}^{alloy}) in Au-Pd alloys as a function of $\log f_{O_2}$. Lines cross-cutting the data divide samples at each temperature containing wüstite (low f_{O_2}) from those containing magnetite (high f_{O_2}). Errors are smaller than the size of the symbol (maximum 2σ values are ±0.2 in $\log f_{O_2}$).

Consider first an Au-Pd-Fe alloy in equilibrium with magnetite. The activity of Fe in the alloy can be calculated using the reaction $3Fe(alloy) + 2O_2(g) = Fe_3O_4(magnetite)$, whose equilibrium constant is given by

$$K_{Mt} = \frac{a_{Fe_3O_4}^{spinel}}{\left(a_{Fe}^{alloy}\right)^3 \left(f_{O_2}\right)^2}. \quad (1)$$

The equilibrium constant, K_{Mt}, was calculated from the expression of O'Neill (1988) for the free energy of formation. Given the equilibrium constant, $\log f_{O_2}$ of the experiment, and the assumption of stoichiometric magnetite (such that $a_{Fe_3O_4}^{spinel} = 1$), the activity of Fe in the alloy can be computed explicitly by rearranging Equation 1 and, given the measured composition of the alloy, the activity coefficient γ_{Fe}^{alloy} can be obtained from $\gamma_{Fe}^{alloy} = a_{Fe}^{alloy}/X_{Fe}^{alloy}$.

The stoichiometry of wüstite varies significantly over the range of oxygen fugacities encompassed by these experiments. Following Kessel et al. (2001), a Gibbs-Duhem integration was performed for the data of Darken and Gurry (1945) via

$$\int_{a_{Fe}^{alloy}@IW}^{a_{Fe}^{alloy}@wüstite} d\ln a_{Fe}^{alloy} = \int_{f_{O_2}@IW}^{f_{O_2}@wüstite} \left(\frac{X_O}{X_{Fe}}\right)^{wüstite} d\ln f_{O_2}^{1/2} \quad (2)$$

where $(X_O/X_{Fe})^{wüstite}$ refers to the molar oxygen-to-iron ratio of the wüstite and integration is taken at the temperature of interest from the IW buffer (where $a_{Fe}^{alloy} = 1$) to the f_{O_2} of interest [for details, see Kessel et al. (2001)]. By integrating from the IW buffer to the oxygen fugacity of an experiment, the activity of Fe in wüstite can be determined and this must be the same as for the Au-Pd-Fe alloy with which it is equilibrated. Calculated activities of Fe for our alloys yield a smooth trend vs. measured alloy composition (Fig. 2) and, in particular, there is no obvious discontinuity between results for magnetite-saturated and wüstite-saturated experiments.

A typical experiment proceeded from low to high concentration of Fe, starting with an Fe-free Au-Pd alloy enclosed in a pellet of hematite. The hematite converted to the stable iron oxide under the run conditions and the alloy equilibrated with that oxide. The identity of the oxide recovered upon quenching was, in all cases, consistent with expectations based on the stability fields for temperature and f_{O_2} for the Fe-O system. Run conditions, identity of run product oxides, and measured alloy compositions are all given in Table 1. A reversal experiment was conducted by first equilibrating an Au-Pd alloy under reducing conditions and quenching (listed as run 7 in Table 1; 1190 °C; $\log f_{O_2} = -11.0$). One alloy strip recovered from this run product

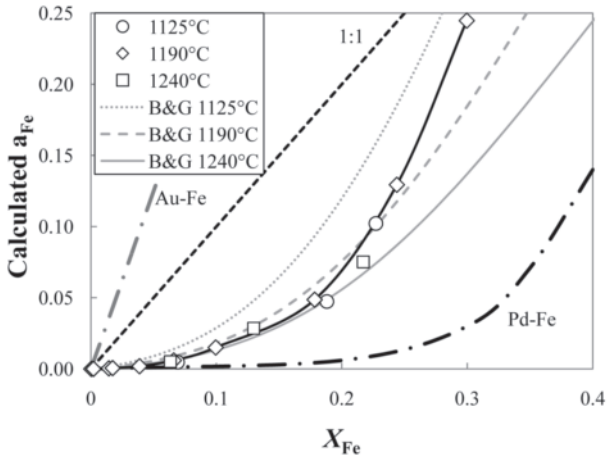

FIGURE 2. Activity of Fe in Au-Pd-Fe alloy relative to elemental Fe, as a function of X_{Fe}^{alloy}. Dashed line is 1:1 line. Solid black curve shows the best fit to our experiments. Labeled dot-dash curves show the relationship for pure Pd-Fe alloys from Ghosh et al. (1999) and Au-Fe alloys from Liu et al. (2009). Gray curves show activity-composition relationships using the calibration of Barr and Grove (2010), labeled as B&G in the legend of this and subsequent figures, calculated for the temperatures of our experiments.

was analyzed (X_{Fe}^{alloy} = 0.30) and the second was placed in a new hematite pellet along with a fresh Fe-free alloy strip and subjected to oxidizing conditions (1190 °C; log f_{O_2} = –3.9). The fresh alloy strip, listed as run 8 in Table 1 yielded Fe three orders of magnitude lower than that obtained for run 7. The second strip, which had previously been exposed to the reducing conditions of run 7 (listed as run 8R in Table 1) now had X_{Fe}^{alloy} ~0.0004 ± 0.0007. This result is consistent with equilibrium, although the uncertainty is high because of the low concentration and because the reversal experiment underwent internal oxidation, leading to precipitation of magnetite within the alloy [Fig. 3b; see e.g., Gegner et al. (2009) for a discussion of internal oxidation of Fe-Pd alloys]. Previously, the identity of all diffusing species in Au-Pd alloys was ambiguous (Truckenbrodt and Johannes 1999) but the internal oxidation observed in run 8R provides clear evidence of oxygen diffusion through the Au-Pd-Fe alloy. This is the only experiment in which internal oxidation was observed and it is presumably a consequence of two factors. First, the concentration of Fe in the alloy exceeded the value for magnetite saturation under the conditions of the experiment (X_{Fe}^{alloy} of the initial alloy = 0.30 >> X_{Fe}^{alloy} at saturation = 0.0003) and second, transport of O into the interior of the alloy was much faster than the transport of Fe out of the interior to the surface [see, e.g., Khanna (2002), for an analysis of internal vs. external oxidation of alloys) perhaps due to the unusually high f_{O_2} of this experiment (4.7 log units above the QFM buffer). The one experiment that exhibited internal oxidation provides insufficient information to delineate the range of conditions over which internal oxidation might be expected to occur, but regardless of the details, supports the idea that oxygen can be transferred across a capsule boundary in high-temperature experiments and that, if this occurs at a sufficiently high rate, the f_{O_2} of an otherwise isolated sample may be altered, even if volatile species such as CO_2 or H_2O are not present as carriers.

Activity-composition model

The Au-Pd-Fe system shows strong negative deviations from ideality for the solution of Fe over the full compositional range examined here; the deviation from ideality decreases with increasing Fe content but the magnitude is generally smaller than that seen in the Pd-Fe system (e.g., Ghosh et al. 1999). The behavior of the Au-Pd-Fe ternary also differs from the Au-Fe binary, which shows positive deviations from ideality across the full composition range (Liu et al. 2009). In principle, it is possible to construct a full thermodynamic model for ternary alloys from data for the bounding binaries, but binaries of the Au-Pd-Fe system are characterized by numerous intermetallic compounds and significant ordering in the fcc solid solution leading to the observed large deviations from ideality (Ghosh et al. 1999; Liu et al. 2009). These features of the system make it difficult to predict ternary solution properties solely from knowledge of the bounding binaries. Attention is restricted to the pseudobinary join along which molar Pd/Au ~0.66 in which the thermodynamic properties have been experimentally determined. It is cautioned that this solution model is applicable only to alloys comparable in composition to the pseudobinary $Au_{60}Pd_{40}$-Fe (molar basis), but this is a common choice of capsule material

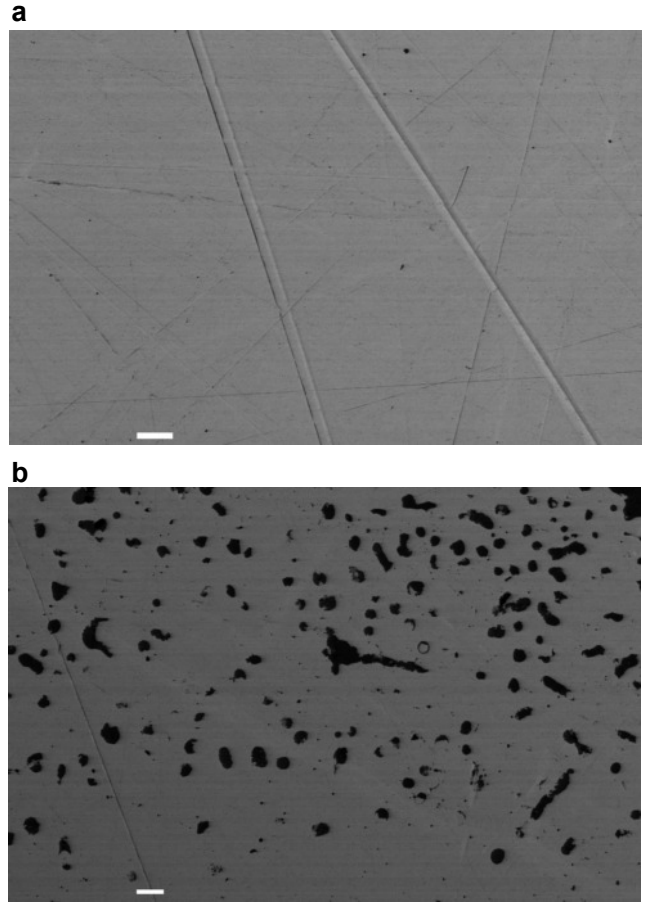

FIGURE 3. Backscattered electron images of runs (**a**) 4 and (**b**) 8R. White bars are 20 µm. Sample 4 (**a**) is typical of run products for our experiments; lines are polishing features and small black spots are dust or specks accumulated on surface. The sample from run 8R (**b**) shows numerous magnetite inclusions (dark splotches) in Au-Pd-Fe alloy.

and so this preliminary calibration should be useful despite the limited composition space.

For a pseudobinary alloy with a composition between fcc Fe and an fcc Au-Pd solution with molar Pd/Au ~0.66, the data is modeled by fitting it to an asymmetric regular solution model of the form

$$RT \ln \gamma_{Fe}^{alloy} = [W_{G\text{-}Fe} + 2(W_{G\text{-}AuPd} - W_{G\text{-}Fe})X_{Fe}^{alloy}](X_{AuPd}^{alloy})^2 \quad (3)$$

$$RT \ln \gamma_{Au\text{-}Pd}^{alloy} = [W_{G\text{-}AuPd} + 2(W_{G\text{-}Fe} - W_{G\text{-}AuPd})X_{AuPd}^{alloy}](X_{Fe}^{alloy})^2 \quad (4)$$

$$X_{Fe}^{alloy} = 1 - X_{AuPd}^{alloy} \quad (5)$$

where γ_i^{alloy} is the activity coefficient of component i in the solution, and W_{Fe} and W_{AuPd} are temperature- and composition-independent Margules parameters. We restrict attention to (X alloy Fe) ≤ 0.3, the upper limit of experimentally observed concentrations, and we use an asymmetric form because the quality of the fit is poor if $W_{G\text{-}Fe} = W_{G\text{-}AuPd}$ is assumed. Temperature independence of the W_G parameters was also assumed because there is no correlation of residuals with temperature over the temperature range examined. Fit values are $W_{G\text{-}Fe} = -45.0 \pm 1.8$ kJ/mol and $W_{G\text{-}AuPd} = +19.5 \pm 7.7$ kJ/mol, consistent with a highly asymmetric solid solution (the quoted 1σ errors were obtained by Monte Carlo simulation, varying all independent and dependent data parameters over Gaussian distributions). All samples in this study show negative deviations from ideal solution, such that the value of $\ln\gamma_{Fe}^{alloy}$ is negative (Fig. 4), although the solution model predicts that at higher values of X_{Fe}^{alloy} (≥0.349), beyond those examined in this study, the value of $RT \ln \gamma_{Fe}^{alloy}$ becomes positive, as is observed in the Pd-Fe system (e.g., Ghosh et al. 1999).

To our knowledge, there are no systematic X-ray data available for ternary Au-Pd-Fe alloys, but Hultgren and Zapffe (1939) and Jette et al. (1934) measured cell volumes for alloys in the Pd-Fe and Au-Fe binaries, both of which show small positive deviations from ideality. Fitting these data to a regular solution model implies W_V values of 0.16–0.17 kJ/(mol GPa) (where $W_G = W_H - TW_S + PW_V$), leading to an increase in W_G by ~0.5 kJ/mol between 1 bar and 3 GPa. This effect is smaller than the 1σ uncertainties on the experimentally determined Margules parameters (1.8 and 7.7 kJ/mol). Thus, available binary volumes are consistent with a negligible pressure effect on the thermodynamic properties, at least up to 3 GPa. The 3 GPa peridotite melting experiments of Balta et al. (in revision) also suggest that excess volumes are small. These authors pre-doped their Au-Pd-Fe capsules based on the 1 atm alloy model with no pressure correction. Had there been a significant pressure effect on the alloy activity-composition relationships, the alloy would have exchanged Fe with the sample to compensate but the capsule composition remained constant within analytical error. We cannot rule out unexpectedly large shifts in γ_{Fe}^{alloy} due to increasing pressures for certain compositions as we did not explicitly measure them, but at present we see no reason to expect a significant pressure effect.

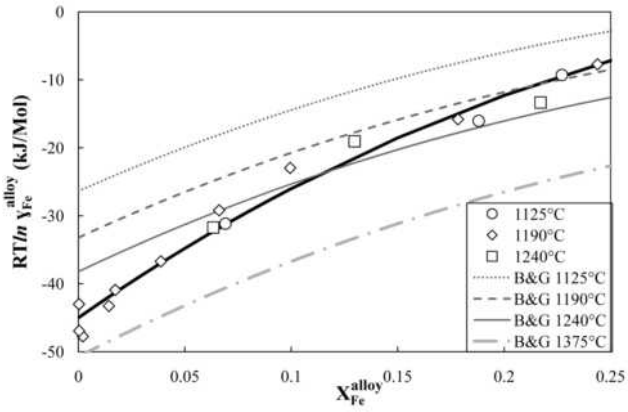

FIGURE 4. $RT \ln \gamma_{Fe}^{alloy}$ as a function of X_{Fe}^{alloy}. 1σ errors given in Table 1 are approximately the same size as the symbols. Black curve is the fit to the regular solution model presented in the text. Gray curves show values calculated using the model of Barr and Grove (2010).

Some notes on the model of Barr and Grove (2010)

In Figures 2 and 4, we show model curves from Barr and Grove (2010), who experimentally approached the thermodynamic properties of Fe-Au-Pd alloys by equilibrating iron-bearing silicate liquids with Au-Pd capsule alloys at various pressures under known temperature and f_{O_2} conditions. These authors modeled their results by: (1) calculating the mole fraction of FeO in the silicate liquid, X_{FeO}^{liq}, using the algorithms of Sack et al. (1980) or Kress and Carmichael (1991) to account for Fe^{2+}/Fe^{3+}; (2) assuming $X_{FeO}^{liq} = a_{FeO}^{liq}$, the activity of FeO in the silicate liquid; (3) constructing a ternary solution model for Au-Pd-Fe alloys from binary Margules parameters derived from literature data; and (4) adding a "misfit parameter" to force agreement with the values of ln K obtained by Médard et al. (2008) based on experiments in that work and in Grove (1981). Their misfit parameter also likely accounts for some of the ternary interactions in Au-Pd-Fe alloys not accounted for through their solution model and errors in the binaries. Barr and Grove's (2010) Au-Pd-Fe model produces activity coefficients in Au-Pd-Fe alloys that are in the general vicinity of our experimentally determined values (Fig. 2) but there are some important differences, most readily seen with the aid of Figure 4. For a given temperature, Barr, and Grove's model predicts $RT \ln \gamma_{Fe}^{liq}$ values as a function of X_{Fe}^{liq} that crosscut our experimental data. This leads to 1 atm predicted values of $RT \ln \gamma_{Fe}^{liq}$ that are too high (1125 °C) or vary from too high to too low as X_{Fe}^{liq} increases (1190 and 1240 °C; this effect can also be seen for high X_{Fe}^{liq} in Fig. 2). Our data show no resolvable temperature dependence for $RT \ln \gamma_{Fe}^{liq}$, but the model of Barr and Grove (2010) predicts a strong temperature dependence, even within the 115° range of our experiments. This leads to model predictions of $RT \ln \gamma_{Fe}^{\circ}$ ($RT \ln \gamma_{Fe}^{liq}$ at infinite dilution) that differ substantially from expectations based on our experimental results, as shown in Figure 4 (–26 kJ/mol at 1125 °C, –33 kJ/mol at 1190 °C, –38 kJ/mol at 1240 °C, and –51 kJ/mol at 1375 °C vs. the experimentally determined value of –45 kJ/mol). Perhaps the most obvious possible causes of these discrepancies are, as noted by Barr and Grove (2010), errors in one or more of the binary thermodynamic models they used to construct a ternary model and/or non-negligible ternary contributions that their model does not take into account. Given the discrepancies apparent in Figure 4, the alloy model of Barr and Grove (2010) should be used with caution in predicting the thermodynamic properties

of ternary Au-Pd-Fe alloy. Barr and Grove's (2010) model may nevertheless be serviceable in the more limited context of Fe partitioning between alloys and silicate liquids.

Preparation and use of Fe-doped Au-Pd capsules for Fe-bearing experiments

Iron-loss to an Au-Pd capsule can lead to significant changes in sample chemistry (e.g., Di Carlo et al. 2006; Dasgupta et al. 2009), which naturally leads to changes in phase equilibria and potentially compromised partition coefficients as phases respond to the changing bulk composition at different rates. In this section, we show how the approach of Kessel et al. (2001) to mitigate Fe-loss in Pt-Fe containers can be adapted to Au-Pd-Fe alloys. The thermodynamics-based MELTS algorithm (Ghiorso and Sack 1995) is used to establish the activity of Fe required for equilibrium with the sample under the conditions of the experiment. The alloy ($Au_{74}Pd_{26}$ by weight)-Fe solution model determined in this work is then used to convert the calculated activity into a desired mole fraction of Fe in the Au-Pd-Fe container and finally into a f_{O_2} value for pre-saturation with the iron oxide. For the liquid components Fe_2SiO_4 and SiO_2, the MELTS algorithm returns values of $\Delta G°$ (an apparent free energy of formation at pressure and temperature referenced to the stable elements at 298.15 K and 1 bar) and the activity in the liquid solution. These can be used to calculate the activity of Fe using the reaction $2Fe_{alloy} + O_2(gas) + SiO_2(liq) = Fe_2SiO_4(liq)$, for which the law of mass action states, at equilibrium,

$$\Delta G = 0 = \Delta G° + RT \ln\left(\frac{a^{liq}_{Fe_2SiO_4}}{a^{liq}_{SiO_2}\left(a^{alloy}_{Fe}\right)^2 f_{O_2}}\right) \quad (7)$$

where ΔG refers to the free energy of reaction and $\Delta G°$ to the standard state free energy of reaction. We corrected the standard state used by MELTS to that of the elements at the temperature of interest using thermodynamic properties of Si, Fe, and O given by Robie et al. (1978) and Equation 15 of Kessel et al. (2001).

We used oxide equilibration at 1 atm to pre-dope Au-Pd-Fe capsules to desired Fe contents for high-pressure experiments, but it is also possible to use silicate liquids for the same purpose. In this approach, the desired Fe content of the alloy under the proposed experimental conditions and volatile contents is first determined as described above (e.g., via MELTS). Then, instead of using oxide equilibration, the Au-Pd capsule is immersed in a large volume of melt at 1 atm using temperature-f_{O_2} conditions calculated to produce the desired Fe content in the alloy. This can be done with starting material or with an arbitrary rock of known composition available in large quantities. As shown in Figure 5a for Kilauea 1919 basalt, it is possible to produce any desired Fe content in the alloy using this basalt by selecting a suitable f_{O_2} and similar diagrams could be produced for other rocks. Following the pre-doping experiment, the melt must be removed, at which point the capsule is ready for use in the desired high-pressure experiment.

The key factors that control how strongly a sample bulk composition will be affected by interaction with an Au-Pd capsule in, for example, a piston-cylinder experiment under high-pressure and high-temperature conditions, are the relative weights of the container and the sample, the initial Fe contents of both, and the Fe activity-composition relationships of the alloy and sample. Pre-doping the container to the Fe content needed to be in equilibrium with the sample under the experimental conditions of interest can substantially reduce exchange between sample and container, but efficacy of the procedure depends on accurate prediction of the desired alloy composition. In the following text, we consider some of the aspects of Au-Pd capsule doping for experiments.

Figure 5a shows a sample calculation of the capsule alloy composition that would be in equilibrium with Kilauea 1919 basalt (Garcia et al. 2003) across a range of oxygen fugacities at 1 bar pressure and 1190 °C [$\log f_{O_2}$ values are presented in terms of differences with respect to the $\log f_{O_2}$ for the quartz-fayalite-magnetite (QFM) buffer]. For f_{O_2} values near QFM, the Fe content of the alloy changes by roughly a factor of 2 for every log unit change in f_{O_2} (Fig. 5b).

A saturation experiment conducted on the Kilauea 1919 basalt ($X^{alloy}_{Fe} = 0.11 \pm 0.01$ at QFM–1.6) shows good agreement with the calculated curve in Figure 5a (see Table 2 for the melt composition and $\Delta G°$ taken from MELTS). Also shown is the

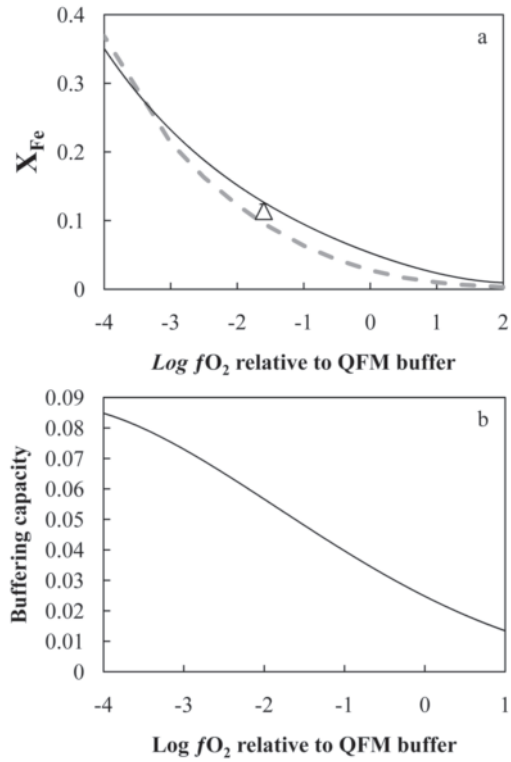

FIGURE 5. (**a**) Calculated compositions of ($Au_{74}Pd_{26}$)-Fe alloys in equilibrium with Kilauea 1919 basalt at 1190 °C and 1 bar as a function of $\log f_{O_2}$ relative to the QFM buffer. The triangle at QFM – 1.6 represents the measured alloy composition experimentally equilibrated with Kilauea 1919 basalt at QFM – 1.6 (measured $X^{alloy}_{Fe} = 0.114$). The error (2σ) is approximately the size of the symbol. The dashed gray curve shows the same calculation using the ternary alloy activity-composition model of Barr and Grove (2010). (**b**) "Buffering capacity" of a capsule in equilibrium with Kilauea 1919 basalt, defined here as the change in the mole fraction of Fe in the capsule per log unit change in oxygen fugacity as a function of $\log f_{O_2}$ relative to the QFM buffer.

alloy composition calculated using the model of Barr and Grove (2010), which agrees equally well with the observed alloy. This result is consistent with expectations based on Figure 4; for $X_{Fe}^{alloy} = 0.11$ and 1190 °C, Figure 4 shows that Barr and Grove's (2010) model predicts values of $RT \ln \gamma_{Fe}^{alloy}$ close to ours [our test experiment was performed prior to publication of Barr and Grove (2010)]. There is clearly a broad swath in temperature – X_{Fe}^{alloy} for which Barr and Grove's (2010) model would yield good predictions of appropriate experimental alloy compositions. For $X_{Fe}^{alloy} = 0.11$, deviations between our model and that of Barr and Grove (2010) are relatively small for temperatures in the range 1200–1250 °C but they increase systematically for lower and higher temperatures.

Unsaturated (i.e., Fe-Free) or incorrectly pre-saturated capsules can cause large shifts in sample composition, but the converse is also true. The presence of an appropriately pre-saturated Au-Pd capsule can provide a strong compositional pseudo-buffer ("pseudo" because the chemical potential of Fe is not in general fixed by the capsule, but if the reservoir of Fe within the capsule is large relative to the sample, it can dramatically reduce shifts in f_{O_2} and Fe content of the sample during an experiment). Moreover, the capsule can act as an indirect monitor of any significant changes in the redox conditions experienced by the sample (Fig. 5) as, under all but the most oxidizing of conditions (or in very low-Fe samples), a single log unit change in f_{O_2} over the course of an experiment should produce significant, readily-measured changes in the composition of the equilibrium alloy and corresponding shifts in the Fe content of the sample. In general, minor mismatches between the f_{O_2} of the prepared sample and the iron content of the capsule will cause the capsule to release or consume Fe until the f_{O_2} of the sample and Fe content of the alloy at the sample-capsule interface are brought close to equilibrium, but at oxygen fugacities where transport of oxygen is faster than Fe as observed in run 8R, or where there are large mismatches between sample and initial alloy, the capsule will fail to act as a pseudo-buffer.

In a typical experiment, the sample is initially loaded as a powder or as small chips, either of which is highly porous prior to heating or pressurization. As a consequence of this high initial porosity and of the higher density and much lower porosity of the capsule compared to the sample, the mass of the capsule is often substantially larger than the mass of the sample. Therefore, given the often high solubility for Fe in an initially Fe-free capsule, very large decreases in sample iron content are likely in the absence of mitigation efforts. For example, Balta et al. (in revision) report a series of water-bearing experiments performed in Au-Pd capsules made from the same stock as the experiments described in this work. In their experiments, the ratio of capsule mass to sample mass ranged from ~3 to ~20, ratios that are typical for common high-pressure experiments. For an Fe-free ~0.3 g Au-Pd capsule loaded with 0.05 g of peridotite containing ~10% FeO, melting experiments produced >60% FeO losses from the phases in the peridotite. By pre-doping the Au-Pd capsules using procedures outlined in this work, run products were produced with limited to no discernable iron loss, despite the extremely high capsule-to-sample mass ratios.

TABLE 2. Composition of Kilauea 1919 basalt in terms of oxides (Garcia et al. 2003) and MELTS components with values for pertinent 1 bar thermodynamic properties at 1190 °C and QFM-1.6 as calculated using the MELTS algorithm

Oxide	wt%	Component	Mole fraction	ΔG^0	Activity*
SiO_2	50.34	SiO_2	0.427457	1040.63	0.461304
TiO_2	2.78	TiO_2	0.02933		
Al_2O_3	13.78	Al2O3	0.128616		
Fe_2O_3	1.01	Fe_2O_3	0.00628		
Cr_2O_3	0.1	$MgCr_2O_4$	0.000653		
FeO	10.08	Fe_2SiO_4	0.069658	1888.07	0.094583
MnO	0.17	$MnSi_{0.5}O_2$	0.00238		
MgO	7.08	Mg_2SiO_4	0.086889		
NiO	0	$NiSi_{0.5}O_2$	0.00004		
CaO	11.5	$CaSiO_3$	0.197753		
Na_2O	2.36	Na_2SiO_3	0.037811		
K_2O	0.53	$KAlSiO_4$	0.011173		
P_2O_5	0.28	$Ca_3(PO_4)_2$	0.001959		

* These activities are used in calculating a_{Fe}^{alloy} via Equation 6 and conversion into X_{Fe}^{alloy} using Equations 3 and 4. The experimentally determined X_{Fe}^{alloy} at QFM-1.6 is 0.114 ± 0.008; the calculated a_{Fe}^{alloy} is 0.021.

Continued refinements and improvements in modeling of Au-Pd-Fe alloys and of the MELTS algorithm will improve the reliability of this calculation. Currently, the pMELTS calibration (Ghiorso et al. 2001) can be used for more accurate calculation of the thermodynamic properties of liquids at pressures up to 3 GPa. Water, in particular, can be expected to have a significant impact on the activities of silica and possibly iron in the liquid phase (e.g., Hirose and Kawamoto 1995; Liu et al. 2006) and thus must be considered in any calculation. The adiabat_1ph front-end for the various MELTS algorithms (Smith and Asimow 2005) can be used to return the thermodynamic parameters in question for liquids calculated by any of the algorithms, and instructions for this process can be obtained from the authors.

ACKNOWLEDGMENTS

The authors thank J.K. Wicks and A.K. Matzen for their help with the 1 atm furnace experiments, and J.H. Jones and T.L. Grove for comments. This work was supported by the NSF Ocean Sciences Marine Geology and Geophysics program, Grant numbers OCE-0241716 and OCE-0550216, and NASA Grant number NNG04GG14G.

REFERENCES CITED

Arndt, N.T. (1976) Melting relations of ultramafic lavas (Komatiites) at 1 atm and high pressure. Carnegie Institution of Washington Yearbook, 75, 555–562.

Aubaud, C., Hirschmann, M.M., Withers, A.C., and Hervig, R.L. (2008) Hydrogen partitioning between melt, clinopyroxene, and garnet at 3 GPa in a hydrous MORB with 6 wt% H_2O. Contributions to Mineralogy and Petrology, 156, 607–625.

Barr, J. and Grove, T. (2010) AuPdFe ternary solution model and applications to understanding the f_{O_2} of hydrous, high-pressure experiments. Contributions to Mineralogy and Petrology, 160, 631–643.

Beckett, J.R. and Mendybaev, R.A. (1997) The measurement of oxygen fugacities in flowing gas mixtures at temperatures below 1200 °C. Geochimica et Cosmochimica Acta, 61, 4331–4336.

Botcharnikov, R.E., Almeev, R.R., Koepke, J., and Holtz, F. (2008) Phase relations and liquid lines of descent in hydrous ferrobasalt—Implications for the Skaergaard intrusion and Columbia River flood basalts. Journal of Petrology, 49, 1687–1727.

Chamberlin, L., Beckett, J.R., and Stolper, E.M. (1994) Pd-oxide equilibration: A new experimental method for the direct determination of oxide activities in melts and minerals. Contributions to Mineralogy and Petrology, 116, 169–181.

Chou, I.-M. (1986) Permeability of precious metals to hydrogen at 2 kb total pressure and elevated temperatures. American Journal of Science, 286, 638–658.

Darken, L.S. and Gurry, R.W. (1945) The system iron-oxygen. I. The wüstite field and related equilibria. Journal of the American Chemical Society, 67, 1398–1412.

Dasgupta, R., Hirschmann, M.M., McDonough, W.F., Spiegelman, M., and Withers, A.C. (2009) Trace element partitioning between garnet lherzolite and carbonatite at 6.6 and 8.6 GPa with applications to the geochemistry of the mantle and of mantle-derived melts. Chemical Geology, 262, 57–77.

Deines, P., Nafziger, R. H., Ulmer, G.C., and Woermann, E. (1974) Temperature-oxygen fugacity tables for selected gas mixtures in the system C-H-O at one atmosphere total pressure. Bulletin of the Earth and Mineral Sciences Experiment Station, Number 88, Pennsylvania State University.

Di Carlo, I., Pichavant, M., Rotolo, S.G., and Scaillet, B. (2006) Experimental crystallization of a high-K arc basalt: the golden pumice, Stromboli Volcano (Italy). Journal of Petrology, 47, 1317–1343.

Dieckmann, R. (1982) Defects and cation diffusion in magnetite (IV): nonstoichiometry and point defect structure of Magnetite ($Fe_{3-\delta}O_4$). Berichte der Bunsen Gesellschaft für Physikalische Chemie, 86, 112–118.

Gaetani, G.A. and Grove, T.L. (1998) The influence of water on melting of mantle peridotite. Contributions to Mineralogy and Petrology, 131, 323–346.

Garcia, M.O., Pietruszka, A., and Rhodes, J.M. (2003) A petrologic perspective of Kilauea volcano's summit magma reservoir. Journal of Petrology, 44, 2313–2339.

Gegner, J., Hörz, G., and Kirchheim, R. (2009) Diffusivity and solubility of oxygen in solid palladium. Journal of Materials Science, 44, 2198–2205.

Ghiorso, M.S. and Sack, R.O. (1995) Chemical mass-transfer in magmatic processes IV. A revised and internally consistent thermodynamic model for the interpolation and extrapolation of liquid-solid equilibria in magmatic systems at elevated temperatures and pressures. Contributions to Mineralogy and Petrology, 119, 197–212.

Ghiorso, M.S., Hirschmann, M.M., Reiners, P.W., and Kress, V.C. (2001) The pMELTS: A revision of MELTS for improved calculation of phase relations and major element partitioning related to partial melting of the mantle to 3 GPa. Geochemistry Geophysics Geosystems, 3, 1030.

Ghosh, G., Kantner, C., and Olson, G.B. (1999) Thermodynamic modeling of the Pd-X (X=Ag, Co, Fe, Ni) systems. Journal of Phase Equilibria, 20, 295–308.

Grove, T.L. (1981) Use of FePt alloys to eliminate the iron loss problem in 1 atmosphere gas mixing experiments: Theoretical and practical considerations. Contributions to Mineralogy and Petrology, 78, 298–304.

Hall, L.J., Brodie, J., Wood, B.J., and Carroll, M.R. (2004) Iron and water losses from hydrous basalts contained in $Au_{80}Pd_{20}$ capsules at high pressure and temperature. Mineralogical Magazine, 68, 75–81.

Harrison, W.J. (1981) Partitioning of REE between minerals and coexisting melts during partial melting of a garnet lherzolite. American Mineralogist, 66, 242–259.

Hirose, K. and Kawamoto, T. (1995) Hydrous partial melting of lherzolite at 1 GPa: The effect of H_2O on the genesis of basaltic magmas. Earth and Planetary Science Letters, 133, 463–473.

Hultgren, R. and Zapffe, C.A. (1939) An X-ray study of the iron-palladium and nickel-palladium systems. Transactions of the American Institute of Mining and Metallurgical Engineers, 133, 58–68.

Iijima, Y. and Yamazaki, B. (2005) Interdiffusion between metals of widely different self-diffusion rates. In M. Danielewski, R. Filipek, R. Kozubs, W. Kucza, P. Zieba, and Z. Zurek, Eds., Diffusion in Materials, Dimat 2004, Pt 1 and 2, 237–240, 62–73. Trans Tech Publications, Zurich-Uetikon.

Jette, E.R., Bruner, W.L., and Foote, F. (1934) An X-ray study of the gold-iron alloys. Transactions of the American Institute of Mining and Metallurgical Engineers, 111, 354–359.

Kägi, R., Muntener, O., Ulmer, P., and Ottolini, L. (2005) Piston-cylinder experiments on H_2O undersaturated Fe-bearing systems: An experimental setup approaching f_{O_2} conditions of natural calc-alkaline magmas. American Mineralogist, 90, 708–717.

Kawamoto, T. and Hirose, K. (1994) Au-Pd sample containers for melting experiments on iron and water bearing systems. European Journal of Mineralogy, 6, 381–385.

Kessel, R., Beckett, J.R., and Stolper, E.M. (2001) Thermodynamic properties of the Pt-Fe system. American Mineralogist, 86, 1003–1014.

Khanna, A.S. (2002) High Temperature Oxidation and Corrosion, 324 p. ASM International, Cleveland, Ohio.

Kress, V. and Carmichael, I. (1991) The compressibility of silicate liquids containing Fe_2O_3 and the effect of composition, temperature, oxygen fugacity and pressure on their redox states. Contributions to Mineralogy and Petrology, 108, 82–92.

Liu, X., O'Neill, H.St.C., and Berry, A.J. (2006) The effects of small amounts of H_2O, CO_2 and Na_2O on the partial melting of spinel lherzolite in the system CaO-MgO-Al_2O_3-SiO_2±H_2O±CO_2±Na_2O at 1.1 GPa. Journal of Petrology, 47, 409–434.

Liu, Y., Ge, Y., and Yu, D. (2009) Thermodynamic descriptions for Au-Fe and Na-Zn binary systems. Journal of Alloys and Compounds, 476, 79–83.

Maestas, S. and Flanagan, T.B. (1973) Diffusion of hydrogen in gold-palladium alloys. Journal of Physical Chemistry, 77, 850–854.

Médard, E., McCammon, C.A., Barr, J.A., and Grove, T.L. (2008) Oxygen fugacity, temperature reproducibility, and H_2O contents of nominally anhydrous piston-cylinder experiments using graphite capsules. American Mineralogist, 93, 1838–1844.

Okamoto, H. and Massalski, T. (1985) The Au-Pd (gold-palladium) system. Journal of Phase Equilibria, 6, 229–235.

O'Neill, H.St.C. (1988) Systems Fe-O and Cu-O: Thermodynamic data for the equilibria Fe-"FeO," Fe-Fe_3O_4, "FeO"-Fe_3O_4, Fe_3O_4-Fe_2O_3, Cu-Cu_2O, and Cu_2O-CuO from emf measurements. American Mineralogist, 73, 470–486.

Robie, R.A., Hemingway, B.S., and Wilson, W.H. (1978) Thermodynamic properties of minerals and related substances at 298.15 K and 1 bar (10^5 Pascals) pressure and at higher temperatures. Geological Survey Bulletin 1452, 456 p.

Sack, R.O., Carmichael, I.S.E., Rivers, M., and Ghiorso, M.S. (1980) Ferric-ferrous equilibria in natural silicate liquids at 1 bar. Contributions to Mineralogy and Petrology, 75, 369–376.

Smith, P.M. and Asimow, P.D. (2005) Adiabat_1ph: A new public front end to the MELTS, pMELTS, and pHMELTS models. Geochemistry Geophysics Geosystems, 6, Q02004.

Truckenbrodt, J. and Johannes, W. (1999) H_2O loss during piston-cylinder experiments. American Mineralogist, 84, 1333–1335.

van Dal, M.J.H., Pleumeekers, M.C.L.P., Kodentsov, A.A., and van Loo, F.J.J. (2000) Intrinsic diffusion and Kirkendall effect in Ni-Pd and Fe-Pd solid solutions. Acta Materialia, 48, 385–396.

Wyllie, P.J. and Tuttle, O.F. (1961) Experimental investigation of silicate systems containing two volatile components. Part II. The effects of NH_3 and HF, in addition to H_2O on the melting temperatures of albite and granite. American Journal of Science, 259, 128–143.

Manuscript received June 25, 2010
Manuscript accepted May 11, 2011
Manuscript handled by Charles Lesher